Accepted Manuscript

Investigation of Advanced Mica Powder Nanocomposite Filler Materials: Surface Energy Analysis, Powder Rheology and Sound Absorption Performance

Lubomír Lapčík, Martin Vašina, Barbora Lapčíková, Eva Otyepková, Kristian Edmund Waters

PII: S1359-8368(15)00175-4

DOI: 10.1016/j.compositesb.2015.03.056

Reference: JCOMB 3490

To appear in: *Composites Part B*

Received Date: 18 February 2015

Accepted Date: 16 March 2015

Please cite this article as: Lapčík L, Vašina M, Lapčíková B, Otyepková E, Waters KE, Investigation of Advanced Mica Powder Nanocomposite Filler Materials: Surface Energy Analysis, Powder Rheology and Sound Absorption Performance, *Composites Part B* (2015), doi: 10.1016/j.compositesb.2015.03.056.

Investigation of Advanced Mica Powder Nanocomposite Filler Materials: Surface Energy Analysis, Powder Rheology and Sound Absorption Performance

Lubomír Lapčík[*1,2], Martin Vašina[3,4], Barbora Lapčíková[1,2], Eva Otyepková[1], Kristian Edmund Waters[5]

[1]Regional Centre of Advanced Technologies and Materials, Department of Physical Chemistry, Faculty of Science, Palacky University, 17. Listopadu 12, 771 46 Olomouc, Czech Republic

[2]Tomas Bata University in Zlin, Faculty of Technology, Inst. Foodstuff Technology, Nam. T.G. Masaryka 275, 760 01 Zlin, Czech Republic

[3]Tomas Bata University in Zlin, Faculty of Technology, Inst. Physics Materials Engineering, Nam. T.G. Masaryka 275, 760 01 Zlin, Czech Republic

[4]VŠB-Technical University of Ostrava, Department of Hydromechanics and Hydraulic Equipment, Faculty of Mechanical Engineering, 17. Listopadu 15/2172, 708 33 Ostrava-Poruba, Czech Republic

[5]Department of Mining and Materials Engineering, McGill University, M.H. Wong Building, 3610 University Street, Montreal, H3A 0C5, Quebec, Canada

[*]Corresponding author. Email: lapcikl@seznam.cz

ABSTRACT

Two types of nano/micro sized mica powders for polymer composites, muscovite and phlogopite, were tested for their sound absorption capabilities. Acoustical performance was correlated to surface energy analysis and powder rheology testing. Inverse gas chromatography (iGC) was used to determine the surface energy, with the dominant

component being the dispersive component. This reflected the non-polar, hydrophobic, character of the micas. The determined yield locus and Mohr´s circles indicated that the material with the highest packing density exhibited more free flowing powder characteristics, compared with the lower packing density materials, which exhibited a greater cohesive powder flow behaviour. All tested mica powders were sensitive to aeration and become fluidised. Based on the acoustical measurements the worst sound absorption performance was found for the highest packing density material exhibiting the highest magnitude of the longitudinal elastic coefficient.

Keywords: *A. Particle-reinforcement; B. Surface properties; B. Rheological properties; B. Physical properties; E. Powder processing.*

1. Introduction

There is a rapidly increasing application of nano particles in most industrial sectors across the globe. Their use is significant benefits to many products, and a large number of research and industrial organisations are attempting to create “nano material” products. The manufacture of large quantities of nano materials, especially in the composite materials market has become a reality and wide range of commercial products can be provided for the global market. Similarly, the surface coatings and paint industries have also started to use available nano materials. Investigations have shown that the size of nano-particle fillers is likely to be the reason behind the performance increase when compared to micrometer sized particles [1,2].

Paint and low temperature coating technologies have moved from a basic chemical process to one where it is now a combination of metallurgy, chemistry and physics, with chemistry at the molecular level approach being now of greatest interest. Typically, colloidal slurry coatings are manufactured for a wide variety of applications, and are used for hard clear coats for

supersonic plastic wind screens, intumescent paints to protect composites, metals and parts such as fuel pumps from fire and erosion coatings for leading edges of wings on sub sonic aircraft. These coatings are also used on: wind turbines, ensuring the longevity of the aerofoil shape; erosion resistant coatings for the leading edges of wings on supersonic aircraft and missiles; erosion coatings on both land based and aeronautical gas turbine parts; in the steel industry for extreme environment protection in the moulds of steel continuous casters; and coatings to down-hole directional drilling mud rotors in the oil industry. High temperature oxidation slurry coatings such as those based on alumina and aluminides are used as overlay barrier coatings in high temperature oxidation applications, dry film lubricants for a wide range of applications, chemical resistant coatings, semiconducting coatings and others. In the last few years, silicate minerals were used in many composite materials technical applications [3]. Incorporating inorganic fillers into thermoplastic/thermosetting polymer networks result in improved physico-chemical, mechanical, and electrical insulation characteristics. For this reason the research and development activities focused on composites containing inorganic filler is of increasing importance. Composite materials matrix modification, its degree of crystallinity, type of reinforcement, quality of adhesion between filler and matrix, filler particles size, size distribution and shape [4,5] as well as the addition of coupling agents enhancing filler/matrix adhesion affects both, the physico-chemical and thermo-mechanical properties, as well as the internal structure and strength of final composites.

The mica group of sheet silicate (phyllosilicate) minerals includes several closely related materials with close to perfect basal cleavage. All are monoclinic, with a tendency towards pseudohexagonal crystals, and are similar in chemical composition. The nearly perfect cleavage, which is the most prominent characteristic of mica, is explained by the hexagonal sheet-like arrangement of its atoms. Chemically, micas can be given the general formula $X_2Y_{4–6}Z_8O_{20}(OH,F)_4$ in which *X* is K, Na, or Ca or less commonly Ba, Rb, or Cs; *Y* is Al, Mg,

or Fe or less commonly Mn, Cr, Ti, Li, etc.; *Z* is chiefly Si or Al, but also may include Fe^{3+} or Ti. As mentioned above, the micas have layer structures in which silicate sheets are combined with aluminate units; the aluminum ions can be octahedrally as well as tetrahedrally coordinated. For example, the mica muscovite $KAl_2(OH)_2(Si_3AlO_{10})$ contains both octahedral and tetrahedral Al^{3+} cations. The potassium ions are located between the fiat aluminosilicate sheets. Phlogopite, $KMg_3(OH)_2(Si_3AlO_{10})$, has a similar structure but with Mg^{2+} in octahedral environments instead of Al^{3+}. The structure and microtopography of mineral filler surfaces are very important because they directly affect surface chemical reaction rates and mechanisms. In general, the surface structure of a mineral differs from the internal structure, however the structure of mineral surfaces may relax due to slight displacements of surface atoms in response to the force asymmetries at the surface or may reconstruct to a surface unit cell of different size and symmetry from that of the equivalent bulk plane [6]. The observed degree of surface relaxation, a consequence of rotation and tilting of SiO_4 tetrahedral after cleaving, is larger in muscovite than in phlogopite. A more tetrahedral rotation after removal of the interlayer K is observed in muscovite. This is due to the greater limitation in the amount of tetrahedral rotation in the internal structure by the interlayer K in muscovite than in phlogopite [6].

This paper focuses on the application of powder rheology, surface energy analysis and acoustical performance testing to evaluate mica powder materials as effective fillers for composite materials applications.

2. **Theoretical background**

2.1. Surface energy analysis

The surface free energy of a solid can be described as the sum of the dispersive and specific contributions. Dispersive (apolar) interactions, also known as Lifshitz-van der Waals

interactions, consist of London interactions which originate from electron density changes but may include both Keesom and Debye interactions [7-9]. The dispersive component of the surface energy (γ_S^D) can be calculated from the retention time of a series of n-alkane probes injected at infinite dilution as measured using inverse gas chromatography (the probe concentration falls within the Henry´s Law portion of the adsorption isotherm) [8,10,11]. There are two methods of determining the surface energy from inverse gas chromatography: the first one isaccording to Schultz et al. [12] (Equation 1*)*; and the second one according to Dorris and Gray [13] *(*Equation 2*)*:

$$RT\ln V_N = a\left(\gamma_L^D\right)^{1/2} 2N_A\left(\gamma_S^D\right)^{1/2} + C \qquad (1)$$

where R is the universal gas constant, N_A is Avogadro´s number, γ_L^D is the dispersive component of surface free energy of the liquid probe, γ_S^D is the dispersive component of the surface free energy of the solid and C is a constant, and

$$\gamma_S^D = \frac{\left[RT\ln\left(V_{N(C_{n+1}H_{2n+4})}\right)/V_{N(C_nH_{2n+2})}\right]}{4N_A^2\, a_{CH_2}^2\, \gamma_{CH_2}} \qquad (2)$$

where a_{CH_2} is the surface area of CH_2 (~0.6 nm^2) and γ_{CH_2} is the free energy of CH_2 (approximately 35.6 mJ/m^2).

2.2. Sound absorption measurements

The ability of a material to absorb incident sound is described by the sound absorption coefficient α, which is given by the ratio [14]:

$$\alpha = \frac{P_d}{P_i} \tag{3}$$

where P_d is the dissipated power in the tested material, and P_i is the incident power. Sound absorption is influenced by many factors, including: excitation frequency; material thickness; porosity; density; and design [15,16]. Frequency dependencies of the sound absorption coefficient of materials can be determined by the transfer function method ISO 10534-2 [17-19]. The complex acoustic transfer function H_{12} is expressed by the formula:

$$H_{12} = \frac{p_2}{p_1} = \frac{e^{k_0 \cdot x_2 i} + r \cdot e^{-k_0 \cdot x_2 i}}{e^{k_0 \cdot x_1 i} + r \cdot e^{-k_0 \cdot x_1 i}} \tag{4}$$

where p_1 and p_2 are the complex acoustic pressures at two microphone positions, k_0 is the complex wave number, x_1 and x_2 are the distances between two microphones and the material sample, r is the normal incidence reflection factor [19], expressed by the following equation:

$$r = r_r + i r_i = \frac{H_{12} - H_I}{H_R - H_{12}} \cdot e^{2k_0 \cdot x_1 i} \tag{5}$$

where r_r and r_i are the real and imaginary parts of the normal incidence reflection factor, H_I is the transfer function for the incident wave, and H_R is the transfer function for the reflection wave. The transfer functions H_I and H_R are defined as follows:

$$H_I = e^{-k_0 \cdot (x_1 - x_2) i} \tag{6}$$

$$H_R = e^{k_0 \cdot (x_1 - x_2) i} \tag{7}$$

The sound absorption coefficient α is then defined by Equation 8:

$$\alpha = 1 - |r|^2 = 1 - r_r^2 - r_i^2 \quad (8)$$

The frequency dependencies of the sound absorption coefficient are experimentally measured using a two-microphone impedance tube. They can subsequently be used for determining the noise reduction coefficient, the speed of sound and the longitudinal elastic coefficient of the studied powder materials.

The noise reduction coefficient (NRC) takes into account an influence of excitation frequency on the sound absorption coefficient. It is defined as the arithmetical average of the sound absorption coefficients of a given material at the excitation frequencies 250, 500, 1000 and 2000 Hz [20-22]:

$$NRC = \frac{\alpha_{250} + \alpha_{500} + \alpha_{1000} + \alpha_{2000}}{4} \quad (9)$$

The speed of sound c of elastic wave through powder beds is proportional to the primary absorption peak frequency f_{p1} as follows [22]:

$$c = 4h\, f_{p1} \quad (10)$$

where h is the height of a given powder bed.

2.3. Calculation of longitudinal elastic coefficient

The longitudinal elastic coefficient K of a powder bed is similar to Young´s modulus of the material. It is proportional to the speed of sound of longitudinal elastic wave and is defined by Equation 11 [22,23]:

$$K = c^2\, \rho_b = \left(4h\, f_{p1}\right)^2 \rho_b \quad , \quad (11)$$

where ρ_b is the bulk density of the powder bed.

The absorption peak frequencies f_p can be in general calculated according to the equation [24]:

$$f_p = \frac{n \cdot c}{4 \cdot h} \qquad (12)$$

where *n* is an odd integer number corresponding to the peak (1 for 1st peak, 3 for 2nd peak, and so on). Because the *c* and *n* are constants, the product of excitation frequency and powder height should also be a constant (Equation 12).

3. Materials

Muscovite mica (sample 1) (Kings Mountains, USA) and phlogopite mica (samples 2 and 3) Suzor type HK325 (Boucherville, Québec, Canada) were used in this study.

4. Methods

4.1. Scanning Electron Microscopy

Scanning electron microscopy (SEM) was used to follow shape and size of the studied mica filler particles. Scanning electron microscopy images were captured on Hitachi 6600 FEG microscope (Japan) operating in the secondary electron mode using an accelerating voltage of 1 kV.

4.2. Thermal Analysis

Thermogravimetry (TG) and differential thermal analysis (DTA) experiments were performed on simultaneous DTA-TG apparatus (Shimadzu DTG 60, Japan). Throughout the experiment, the sample temperature and weight-heat flow changes were continuously monitored. The measurements were performed at heat flow rate of 10°C/min in the static air atmosphere at the temperature range of 30°C to 300°C.

4.3. Specific surface area and porosity analysis

Specific surface area measurements were made using Micromeritics TriStar 3000 surface area and porosity analyser (USA) combined with the nitrogen BET technique.

4.4. Surface Energy Analysis (SEA)

Inverse gas chromatography was conducted using a surface energy analyser (SEA) (Surface Measurement Systems, UK). Samples were placed in 4 mm (internal diameter) columns to give a total surface area of approximately 0.5 m^2. The following eluent vapours were passed through the column: nonane, octane, hexane, heptane, dichloromethane, acetone, acetonitrile, ethyl acetate and ethanol. All reagents were obtained from Sigma Aldrich (USA) and were of analytical grade. The injection of vapours was controlled in order to pass a set volume of eluent through the column to give pre-determined fractional coverage of the sample in the column. Using this method, the retention time of the vapours through the particles gives an indication of the surface properties of the material, including the surface energy. By gradually increasing the amount of vapour injected, it is possible to build up a surface heterogeneity plot.

4.5. Powder rheology

Powder rheology measurements were conducted on a FT4 Powder rheometer (Freeman Technology, UK). All experiments were performed under the ambient laboratory temperature of 23 °C and relative humidity of 43 %.

4.6. Acoustical performance testing

The impedance tube method for sound absorbing testing based on transfer function method ISO 10534-2 standard was used. The frequency dependencies of the sound absorption coeffi**c**ient were experimentally measured using a two-microphone impedance tube (BK

4206) in combination with three-channel signal PULSE multi-analyser (BK 3560-B-030) and power amplifier (BK 2706) in the frequency range of 150-6400 Hz (Brüel & Kjær, Denmark). The normal incidence sound wave absorption of the tested loose powder samples of defined layer thickness (ranging from 2.5 to 100 mm) was determined. All experiments were performed under ambient laboratory conditions of 40 % relative humidity and at 22°C.

Results and discussion

As mentioned previously, inorganic nano/micro particles are used as intelligent fillers in many polymer based composites, as well as in the paper and dye industries [1-4,25-28]. The dominant factors are: particle uniformity; diameter; surface chemistry [29]; and shape, which influences the physical and material properties of the final product. These properties include mechanical strength, thermal behaviour, barrier properties, and electrical conductivity. As shown in Figure 1, the mica nano/micro powders exhibit typical a plate-like planar structure. As observed by SEM analysis, the mica particles had a thickness of approximately 150 nm. The specific surface areas of the studied samples were identical (9.67 m^2/g) for all materials under study. Due to the fact that residual captured moisture from the ambient atmosphere strongly affects the surface energy and powder rheological behaviour, prior to these experiments the water content in all samples was characterized by means of thermal analysis across the temperature range of 30 to 300°C. There were found no traces of any kind of free water molecules at the surface as well as in crystal lattice of the powders under study. As confirmed by previous studies, the surface chemistry of the fillers affects the contacts at the filler/matrix interface, which are paramount for obtaining a final composite with the desired mechanical properties [1,2]. The chemical composition reflects the crystal structure of the filler, and on a macroscopic scale it influences polarity, thus the wetting characteristics. In this study, as shown in Figure 2, inverse gas chromatography was used to determine the surface

energy [8] and to quantify the surface energy profiles and its components (polar and dispersive parts) as a function of surface coverage. Here a typical exponential decrease of total surface energy of for all studied samples was observed up to the 0.3 surface coverage reflecting thus relatively broad number of high energy sites in the studied materials. The highest energy sites were of 85 mJ/m^2 total surface energy for the muscovite (sample 1), followed by the two phlogopite samples, sample 3 (78 mJ/m^2) and sample 2 (75 mJ/m^2). For surface coverage exceeding 30 % the total surface energy was practically constant ranging between 52 mJ/m^2 for the sample 1 up to 57 mJ/m^2 for the sample 3. As evident from the Figure 2, dominating was dispersive component of the surface energy as compared to the polar component for all studied powders thus reflecting non-polar hydrophobic character. The hydrophobic character of muscovite micas has been observed by AFM experiments, where the high adhesion observed for the interaction between the hydrophobic $-CH_3$ tip and muscovite was caused by van der Waals forces and attractive hydrophobic interactions that originate from the inherent hydrophobicity and adventitious carbon present on the solid surface [30]. In the case of the polar surface energy component, the difference between the highest and the lowest energy sites was approximately 6 mJ/m^2 showing an exponential decrease similar to that of the total and dispersive components. The maximum value of the polar part of the surface energy observed for the muscovite was approximately 15 mJ/m^2. The measured dispersive surface energy (Figure 3), showed a characteristically relatively broad distribution for both the muscovite (44 mJ/m^2 to 84 mJ/m^2), and the phlogopite, samples 2 (46 mJ/m^2 to 76 mJ/m^2) and 3 (48 mJ/m^2 to 88 mJ/m^2), thus reflecting relatively large number of structural elements which might be responsible for this behaviour. In contrast, the area increment occupancy for the sample 3 was approximately two times higher, reaching 1.3 % in comparison with the sample 1 (0.6 %) and the sample 2 (0.8 %).

The flow properties of bulk solids depend on many parameters, e.g. particle size distribution, particle shape, chemical composition of the particles, moisture content, temperature [7] as well as on experimental conditions [31-33]. The macroscopic powder flow behaviour was also investigated in this study by determining the yield locus and flow function dependencies at different stress levels applied on the studied samples. Results of the powder rheological measurements are shown in Figure 4, which presents the yield locus and Mohr´s circles of the tested mica powders. The results show that the muscovite exhibited easy flowing powder characteristics, as indicated by the observed flowability of 8.4, which is relatively close to the region of free flowing powders. In contrast, the flowabilities of the phlogopite samples ranged from 5.44 to 5.53, which are values characteristic for easy flowing powders behaviour, however near to the cohesive region. The unconfined yield strengths ranged from 2.54 kPa (sample 1) to 3.54 kPa (sample 2) and 2.89 kPa (sample 3). The angle of internal friction ranged from 29.3° for the sample 3 up to 35.1 and 39.9° for the sample 2 and the sample 1, respectively. The relevant consolidation stress, $\sigma_{1,}$ can be obtained from the major principal stress of the Mohr stress circle tangential to the yield locus and intersecting the point of steady flow. The major principle stress for all the tested powders was about 16 to 21.4 kPa. The latter stress circle represents the stresses in the sample at the end of the consolidation procedure (stress at steady state flow). It corresponds to the stress circle at the end of consolidation in the uniaxial compression test. The bulk density of the powders in general depends on the state of compaction of the bulk solid. The latter state of compaction depends on applied magnitude of the consolidation stress acting on the bulk solid during powder testing. Under the experimental conditions used in this work (preshear normal stress of 9 kPa), the observed samples bulk densities ranged from 0.405 g/ml for phlogopite (sample 3) to 0.451 g/ml (muscovite, sample 1). This shows that the cohesive character of the phlogopite triggers a less compact solid-like structure than the muscovite. This conclusion is in excellent agreement

with aeration data shown in Figure 5. The aeration ratio was found to range from 21.8 for the phlogopite (sample 2) to 38.4 for the muscovite (sample 1), whereas the aerated energy varied from 4.18 mJ (sample 3) to 7.49 mJ (sample 1). The aeration data indicated that the muscovite showed the lowest cohesion of all the samples tested. However, all three mica powders were sensitive to aeration and become fluidised. The phlogopite powders exhibited complete fluidisation at 2 mm/s air velocity, with basic flowability energy approximately 93 mJ. This is in contrast to the muscovite, which exhibited complete fluidisation at 6 mm/s air velocity, with a basic flowability energy of 288 mJ, thus supporting the conclusion of low cohesive powder character.

Sound damping properties of the materials are in general strongly affected by the porosity, shape of the pores and friction coefficient of the incident air in the pores, the material mechanical stiffness as well as on the conditions of the applied dynamic acoustic field as given by the frequency and amplitude of the vibration field [16]. This is why, to some extent, the cohesive character of the powder samples would affect their acoustic performance. Due to the relative complexity of the sound wave interaction with the incident material surface layer as well as penetrated material inner structure, factors such as incident sound wave angle and sound wave frequency would also influence final acoustic impedance frequency dependency. Results of our normal incidence sound absorption experiments are shown in Figure 6 and are summarised in Table 1. In general, the sound absorption efficiency increases with increasing material thickness, in this case with height of the loose powder bed. Figure 6 shows the data for phlogopite (sample 2). Observed frequency dependencies of the normal incident sound absorption coefficient were characteristic with the appearance of the primary absorption peak at a characteristic frequency f_{p1}. The latter primary absorption peak frequency was shifted toward decreasing frequency with increasing powder bed height (Figure 7), i.e. for the bed height of 10 mm the frequency f_{p1} was located at 648 Hz having the sound absorption

coefficient 0.59 (sample 2). For 100 mm sample 2 powder bed height the frequency f_{p1} was located at 224 Hz having the sound absorption coefficient 0.53. No primary sound absorption peak was observed below 200 Hz frequency for any of the samples studied. Homogeneous porous materials containing interconnecting pores exhibit two types of sound absorption mechanisms: the first type is due to the air friction passing through the powder bed pores, the second one is due to the mechanical vibration of the solid structure of the powder bed [22]. The sound absorption coefficient of the first type is low at low frequencies and high at high frequencies. In contrary to the latter frequency behaviour the second type of sound absorption is giving rise to a high absorption coefficient at the resonant frequencies of the solid structure, in our case when the size of the pores becomes relatively small and resistance to air flow is high. As shown in Figure 6, the observed sound absorption coefficient frequency dependencies exhibited primary as well as secondary (and higher) sound absorption peaks for all materials. Calculated frequencies for all samples under study having minimum powder bed height of 7.5 mm up to 30 mm exhibited the ratio of secondary absorption peak frequency/primary peak frequency of approximately 3. This value is in excellent agreement also with the Equation 12. This confirmed that the latter resonant vibration modes are considered to be the one-end fixed longitudinal modes [22]. The appearance of the primary sound absorption peaks at the same frequency can be confirmed, as shown in Figure 7. This result confirms that the product of frequency and powder bed height plotted against the sound absorption coefficient dependency was constant, irrespective of the specimen powder bed height according to Equation 12 [24]. This behaviour is consistent with the fact that c and n were constants. Based on the acoustic measurements the worst sound absorption performance was found for the muscovite across a substantial part of the measured frequency range. This conclusion is in excellent agreement with the observed the lowest magnitude of the noise reduction coefficient NRC (Equation 9) for all tested powder bed heights (see Table 1, data

for muscovite). In the case of powder bed height in the range of 2.5 mm up to 30 mm the best sound absorbing properties were found for the sample 2, in the case of the *h* exceeding 50 mm the best noise damping properties were observed for the sample 3. To confirm this, calculations of the longitudinal elastic coefficient *K* of the powder bed according to Equation 11 were performed [22]. As expected, due to the densest structure of the powder bed found for the sample 1 (0.451 g/ml observed bulk density from powder rheology), the worst acoustic performance was found accompanied by the highest elastic coefficient magnitude of 3.37 MPa (for h = 100 mm). The lowest *K* was found for the sample 3 of 3.02 MPa (see Table 1). This result is in excellent agreement with the observed lowest value of the angle of internal friction of 29.3° for the sample 3 which was characteristic for cohesive powders. Calculated speed of sound (eq. (10)) of the elastic wave propagated through the powder bed (of h = 30 mm) was highest for sample 1 (c = 33.6 m/s) due to the most dense structure in comparison with the more aerated porous structure of the sample 2 (c = 32.6 m/s) and the sample 3 (c = 32.6 m/s) powders.

Conclusions

It was found in this study that the combination of the results of the surface energy analysis performed by iGC, correlated with the powder rheology testing, can be used for the evaluation of the acoustical performance of the studied powder materials. It was found that the application of a combination of the two mode dissipation mechanisms of sound wave propagation in the powder bed is correct, the first based on sound energy dissipation due to the internal friction of the sound wave in the porous solid structure of the solid in combination with the sound absorption due to the vibration of the solid structure. Based on surface energy analysis, the dispersive component of the surface energy was the dominant component for all studied powders, thus reflecting non-polar hydrophobic character of the materials tested. In

the case of the polar surface energy component the difference between the highest and the lowest energy sites was only about 6 mJ/m^2. Maximum values of the polar part of the surface energy observed for muscovite was approximately 15 mJ/m^2. There was found more cohesive character of the phlogopite compared to the muscovite, which triggers a less compact solid like structure in the case of the sample 1. Mechanical testing of powder beds was performed by means of powder rheology. The determined yield locus and Mohr´s circles indicated that the muscovite exhibited more free flowing powder characteristics, whereas the phlogopite samples exhibited more cohesive powder flow behaviour. This conclusion was confirmed by aeration tests. All mica powders were sensitive to aeration and became fluidised. Observed frequency dependencies of the normal incident sound absorption coefficient were characteristic with appearance of the primary absorption peak at characteristic frequency f_{p1}. The latter primary absorption peak frequency was shifted toward decreasing frequency with increasing powder bed height. Based on the acoustical measurements the worst sound absorption performance was found for the muscovite in a substantial part of the measured frequency range. This conclusion was in excellent agreement with the observed the lowest magnitude of the noise reduction coefficient NRC for all tested powder bed heights. Calculation of the longitudinal elastic coefficient K of each powder bed was performed. The worst acoustic performance was found for the muscovite, which corresponded to the observed highest elastic coefficient of 3.37 MPa (for h = 100 mm). The lowest K was found to be 3.02 MPa (phlogopite sample 3), in excellent agreement with powder rheology measurements.

Acknowledgements

Financial support from the grant no. LO1305 of the Ministry of Education, Youth and Sports of the Czech Republic is gratefully acknowledged. Authors would like to express their gratitude for SEM measurements to Dr. K. Čépe (Palacky University in Olomouc).

References

[1] Lapčík L, Jindrová P, Lapčíková B, Tamblyn R, Greenwood R, Rowson N. Effect of the Talc Filler Content on the Mechanical Properties of Polypropylene Composites. J Appl Polym Sci 2008;110(5):2742-2747.

[2] Krásny I, Lapčík L, Lapčíková B, Greenwood RW, Safářová K, Rowson NA. The effect of low temperature air plasma treatment on physico-chemical properties of kaolinite/polyethylene composites. Composites Part B-Engineering 2014;59:293-299.

[3] Martias C, Joliff Y, Favotto C. Effects of the addition of glass fibers, mica and vermiculite on the mechanical properties of a gypsum-based composite at room temperature and during a fire test. Composites Part B-Engineering 2014;62:37-53.

[4] Andric L, Terzic A, Acimovic-Pavlovic Z, Pavlovic L, Petrov M. Comparative kinetic study of mechanical activation process of mica and talc for industrial application. Composites Part B-Engineering 2014;59:181-190.

[5] Andric L, Terzic A, Acimovic-Pavlovic Z, Trumic M, Petrov M, Pavlovic L. A Kinetic Study of Micronization Grinding of Dry Mica in a Planetary Ball Mill. Advances in Materials Science and Engineering 2013:543857.

[6] Kuwahara Y. Comparison of the surface structure of the tetrahedral sheets of muscovite and phlogopite by AFM. Physics and Chemistry of Minerals 2001;28(1):1-8.

[7] Lapčík L, Lapčíková B, Krásny I, Kupská I, Greenwood RW, Waters KE. Effect of Low Temperature Air Plasma Treatment on Wetting and Flow Properties of Kaolinite Powders. Plasma Chem Plasma Process 2012;32(4):845-858.

[8] Mohammadi-Jam S, Waters KE. Inverse gas chromatography applications: A review. Adv Colloid Interface Sci 2014;212:21-44.

[9] Gajdošíková R, Lapčíková B, Lapčík L. Surface phenomena and wetting of porous solids. Phys Chem : Indian J 2011;6(3):146-162.

[10] Mohammadi-Jam S, Burnett DJ, Waters KE. Surface energy of minerals - Applications to flotation. Minerals Eng 2014;66-68:112-118.

[11] Ali SSM, Heng JYY, Nikolaev AA, Waters KE. Introducing inverse gas chromatography as a method of determining the surface heterogeneity of minerals for flotation. Powder Technol 2013;249:373-377.

[12] Schultz J, Lavielle L, Martin C. The Role of the Interface in Carbon-Fiber Epoxy Composites. J Adhesion 1987;23(1):45-60.

[13] Dorris GM, Gray DG. Adsorption of Normal-Alkanes at Zero Surface Coverage on Cellulose Paper and Wood Fibers. J Colloid Interface Sci 1980;77(2):353-362.

[14] Sgard F, Castel F, Atalla N. Use of a hybrid adaptive finite element/modal approach to assess the sound absorption of porous materials with meso-heterogeneities. Appl Acoust 2011;72(4):157-168.

[15] Vašina M, Hughes DC, Horoshenkov KV, Lapčík L. The acoustical properties of consolidated expanded clay granulates. Appl Acoust 2006;67(8):787-796.

[16] Lapčík L, Cetkovský V, Lapčíková B, Vašut S. Materials for noise and vibration attenuation. Chem Listy 2000;94(2):117-122.

[17] Han FS, Seiffert G, Zhao YY, Gibbs B. Acoustic absorption behaviour of an open-celled aluminium foam. Journal of Physics D-Applied Physics 2003;36(3):294-302.

[18] Cheerier O, Pommier-Budinger V, Simon F. Panel of resonators with variable resonance frequency for noise control. Appl Acoust 2012;73(8):781-790.

[19] International Standard ISO 10534-2:1998. Acoustics-Determination of sound absorption coefficient and impedance in impedance tubes-Part 2: Transfer-function method.

[20] Buratti C. Indoor Noise Reduction Index with an open window (Part II). Appl Acoust 2006;67(5):383-401.

[21] Tiwari V, Shukla A, Bose A. Acoustic properties of cenosphere reinforced cement and asphalt concrete. Appl Acoust 2004;65(3):263-275.

[22] Okudaira Y, Kurihara Y, Ando H, Satoh M, Miyanami K. Sound-Absorption Measurements for Evaluating Dynamic Physical-Properties of a Powder Bed. Powder Technol 1993;77(1):39-48.

[23] Yanagida T, Matchett AJ, Coulthard JM, Asmar BN, Langston PA, Walters JK. Dynamic measurement for the stiffness of loosely packed powder beds. AIChE J 2002;48(11):2510-2517.

[24] Marolf A, Neithalath N, Sell E, Wegner K, Weiss J, Olek J. Influence of aggregate size and gradation on acoustic absorption of enhanced porosity concrete. ACI Mater J 2004;101(1):82-91.

[25] Doost-hoseini K, Taghiyari HR, Elyasi A. Correlation between sound absorption coefficients with physical and mechanical properties of insulation boards made from sugar cane bagasse. Composites Part B-Engineering 2014;58:10-15.

[26] El-Sabbagh A, Steuernagel L, Ziegmann G. Characterisation of flax polypropylene composites using ultrasonic longitudinal sound wave technique. Composites Part B-Engineering 2013;45(1):1164-1172.

[27] Huda S, Reddy N, Yang Y. Ultra-light-weight composites from bamboo strips and polypropylene web with exceptional flexural properties. Composites Part B-Engineering 2012;43(3):1658-1664.

[28] Hořáková V, Tomeček P, Lapčík L, Greenwood R. The effect of surface modification on the zeta potential and the stability of calcium pyrophosphate powders. Journal of Polymer Materials 2005;22(4):385-389.

[29] Greenwood R, Lapčíková B, Surýnek M, Waters K, Lapčík L. The zeta potential of kaolin suspensions measured by electrophoresis and electroacoustics. Chemical Papers 2007;61(2):83-92.

[30] Juhl KMS, Pedersen CS, Bovet N, Dalby KN, Hassenkam T, Andersson MP, Okhrimenko D, Stipp SLS. Adhesion of Alkane as a Functional Group on Muscovite and Quartz: Dependence on pH and Contact Time. Langmuir 2014;30(48):14476-14485.

[31] Schulze D, Wittmaier A. Flow properties of highly dispersed powders at very small consolidation stresses. Chem Eng Technol 2003;26(2):133-137.

[32] Schulze D, Wittmaier A. Measuring the flow properties of highly disperse bulk solids at very small consolidation strains. Chemie Ingenieur Technik 2002;74(8):1144-1148.

[33] Jenike AW. Measure of flowability for powders and other bulk solids. Powder Technol 1975;11(1):89-90.

Figure chapter

Figure 1. SEM images of studied mica powders: A) sample 1, B) sample 2, and C) sample 3.

Figure 2. Surface energy and its component profiles of mica powders: circle – sample 1, triangle – sample 2, crosshair – sample 3, black– dispersive component of the surface energy (SFE), red – polar component of SFE, green colour – total SFE. (For interpretation of the references to colour in this figure legend, the reader is referred to the web version of this article).

Figure 3. Dispersive surface energy distribution of studied mica powder: sample 1 (circle), sample 2 (triangle) and sample 3 (crosshair).

Figure 4. Yield locus and Mohr´s circles of studied mica powders (measured at 24 °C).

Figure 5. Aeration test results for studied mica powders (measured at 24 °C).

Figure 6. Sound absorption coefficient frequency dependence of the mica powder sample 2 as observed for different loose unconsolidated powder layer thickness given in millimetres (see the insert legend). (For interpretation of the references to colour in this figure legend, the reader is referred to the web version of this article).

Figure 7. Dependence of the primary absorption peak frequency (f_{p1}) vs. loose powder layer thickness of the studied mica powders: sample 1 (circle), sample 2 (triangle) and sample 3 (crosshair). Inset: Illustration for sample 2 of the sound absorption coefficient (α) dependence on product of frequency × thickness ($f \times h$) being constant irrespective of specimen thickness. Inserted inset legend: loose powder thickness in millimetres. (For interpretation of the references to colour in this figure legend, the reader is referred to the web version of this article).

Table chapter

Table 1. Results of the calculated and measured acoustical and mechanical quantities of studied mica powders.

Table 1. Results of the calculated and measured acoustical and mechanical quantities of studied mica powders.

Sample No.	Quantity	Material height h [mm]										
		2.5	5	7.5	10	12.5	15	20	30	40	50	100
1	α_{max} [–]	0.440	0.689	0.499	0.558	0.506	0.534	0.518	0.636	0.618	0.637	0.573
	$f_{\alpha max}$ [Hz]	6352	6400	6182	6184	608	464	344	6400	240	240	5736
	NRC [–]	0.054	0.166	0.198	0.233	0.237	0.235	0.222	0.227	0.318	0.370	0.261
	f_{p1} [Hz]	–	1360	1064	744	608	464	344	280	240	240	216
	K [MPa]	–	0.334	0.460	0.399	0.417	0.350	0.342	0.509	0.665	1.039	3.367
	c [m·s^{-1}]	–	27.2	31.9	29.8	30.4	27.8	27.5	33.6	38.4	48.0	86.4
2	α_{max} [–]	0.495	0.714	0.593	0.585	0.655	0.784	0.727	0.766	0.633	0.619	0.672
	$f_{\alpha max}$ [Hz]	6392	5560	5848	648	6368	6400	6400	6400	5688	240	6400
	NRC [–]	0.108	0.196	0.219	0.238	0.273	0.286	0.269	0.294	0.369	0.389	0.312
	f_{p1} [Hz]	–	–	1128	648	560	472	352	272	248	240	224
	K [MPa]	–	–	0.472	0.277	0.323	0.330	0.327	0.439	0.649	0.949	3.308
	c [m·s^{-1}]	–	–	33.8	25.9	28.0	28.3	28.2	32.6	39.7	48.0	89.6
3	α_{max} [–]	0.509	0.571	0.588	0.619	0.612	0.653	0.754	0.716	0.658	0.809	0.787
	$f_{\alpha max}$ [Hz]	6392	6392	936	680	544	6400	6400	6400	6344	6400	6400
	NRC [–]	0.077	0.174	0.216	0.200	0.274	0.269	0.265	0.296	0.352	0.397	0.290
	f_{p1} [Hz]	–	1680	936	680	544	464	352	272	264	248	216
	K [MPa]	–	0.457	0.319	0.300	0.300	0.314	0.321	0.431	0.723	0.996	3.023
	c [m·s^{-1}]	–	33.6	28.1	27.2	27.2	27.8	28.2	32.6	42.2	49.6	86.4

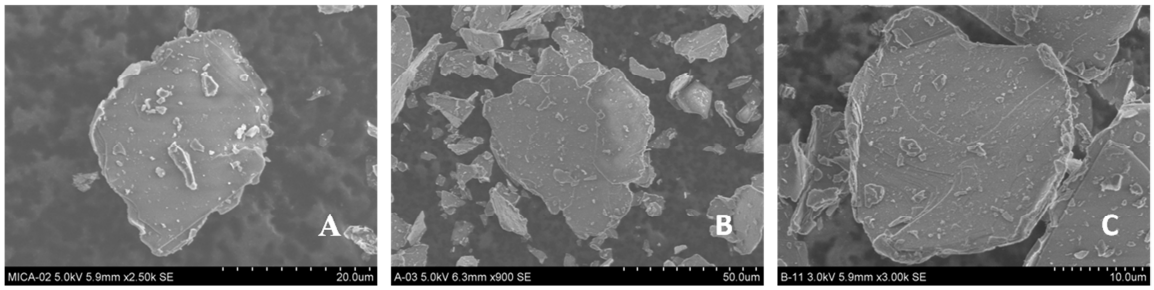

Figure 1. SEM images of studied mica powders: A) sample 1, B) sample 2, and C) sample 3.

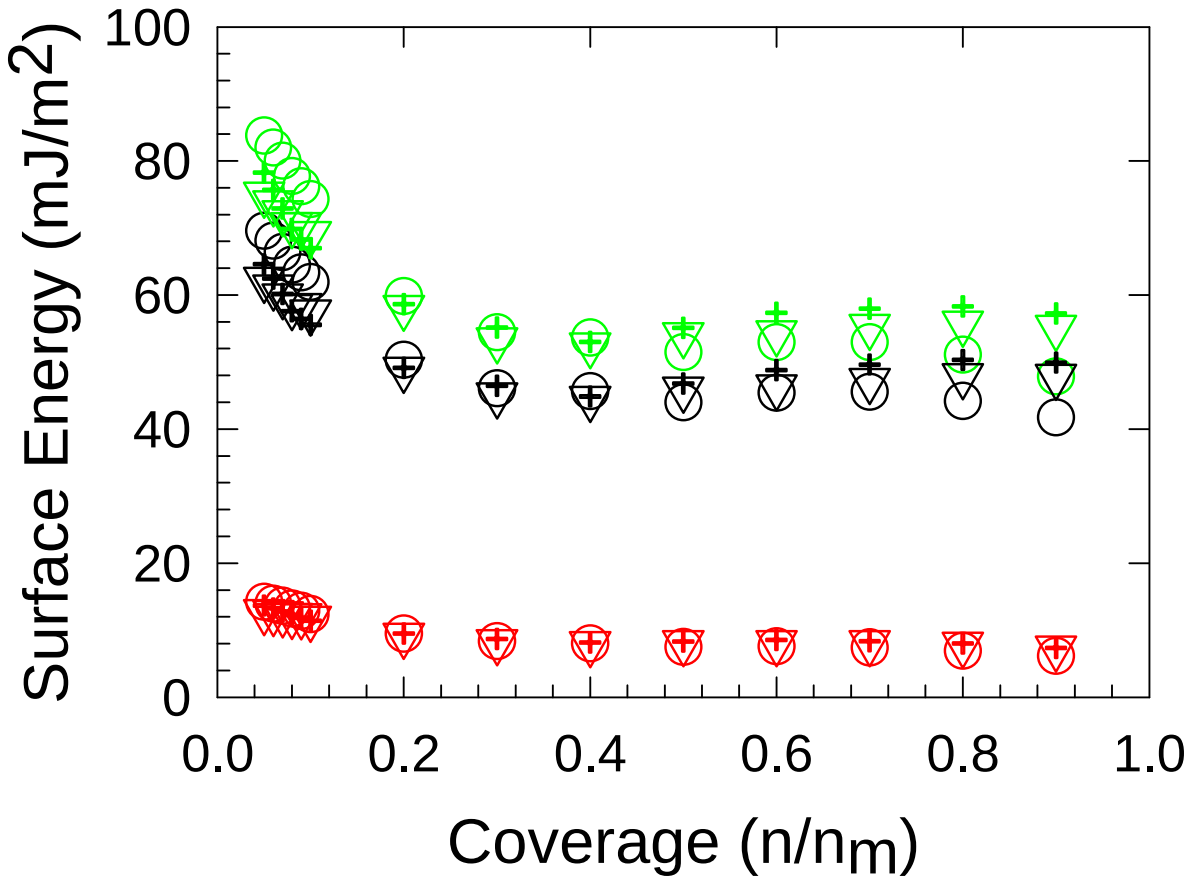

Figure 2. Surface energy and its component profiles of mica powders: circle – sample 1, triangle – sample 2, crosshair – sample 3, black– dispersive component of the surface energy (SFE), red – polar component of SFE, green colour – total SFE. (For interpretation of the references to colour in this figure legend, the reader is referred to the web version of this article).

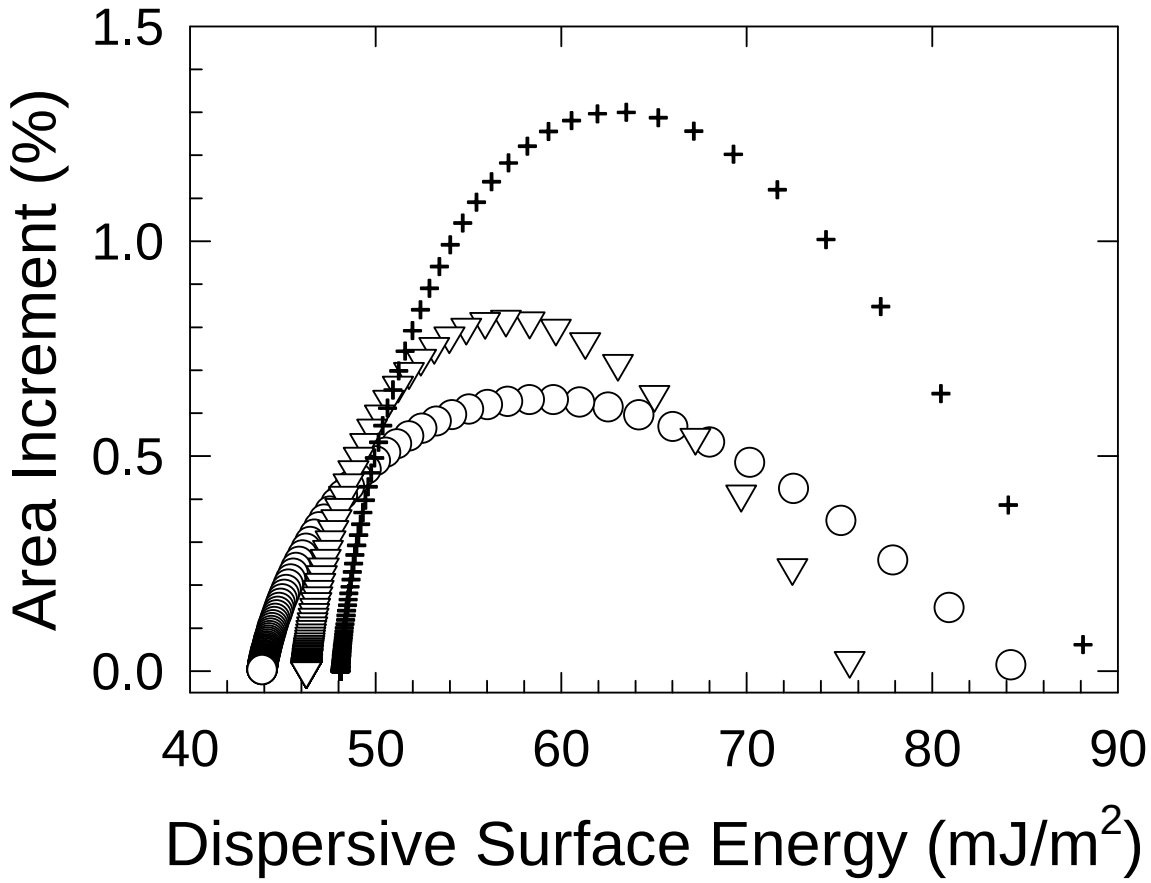

Figure 3. Dispersive surface energy distribution of studied mica powder: sample 1 (circle), sample 2 (triangle) and sample 3 (crosshair).

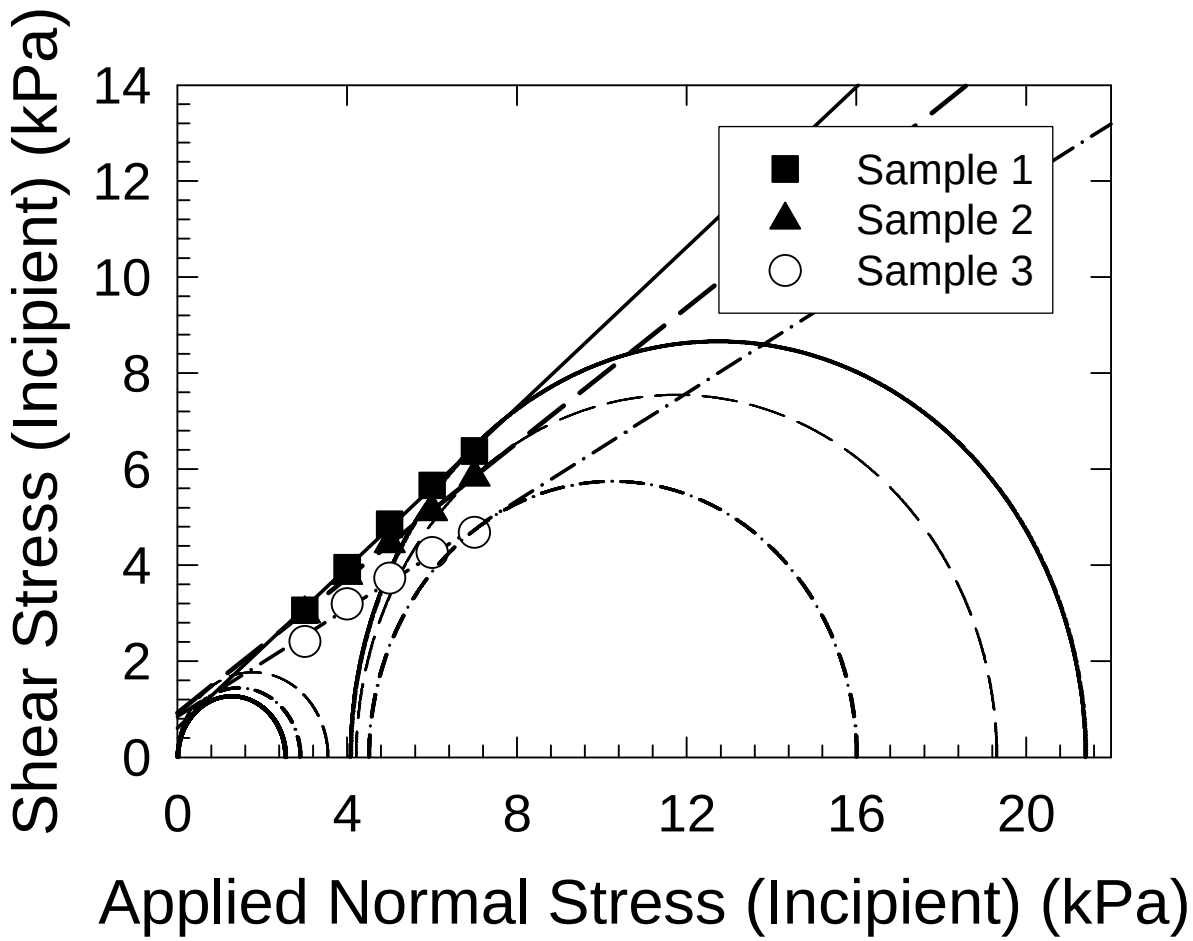

Figure 4. Yield locus and Mohr´s circles of studied mica powders (measured at 24 °C).

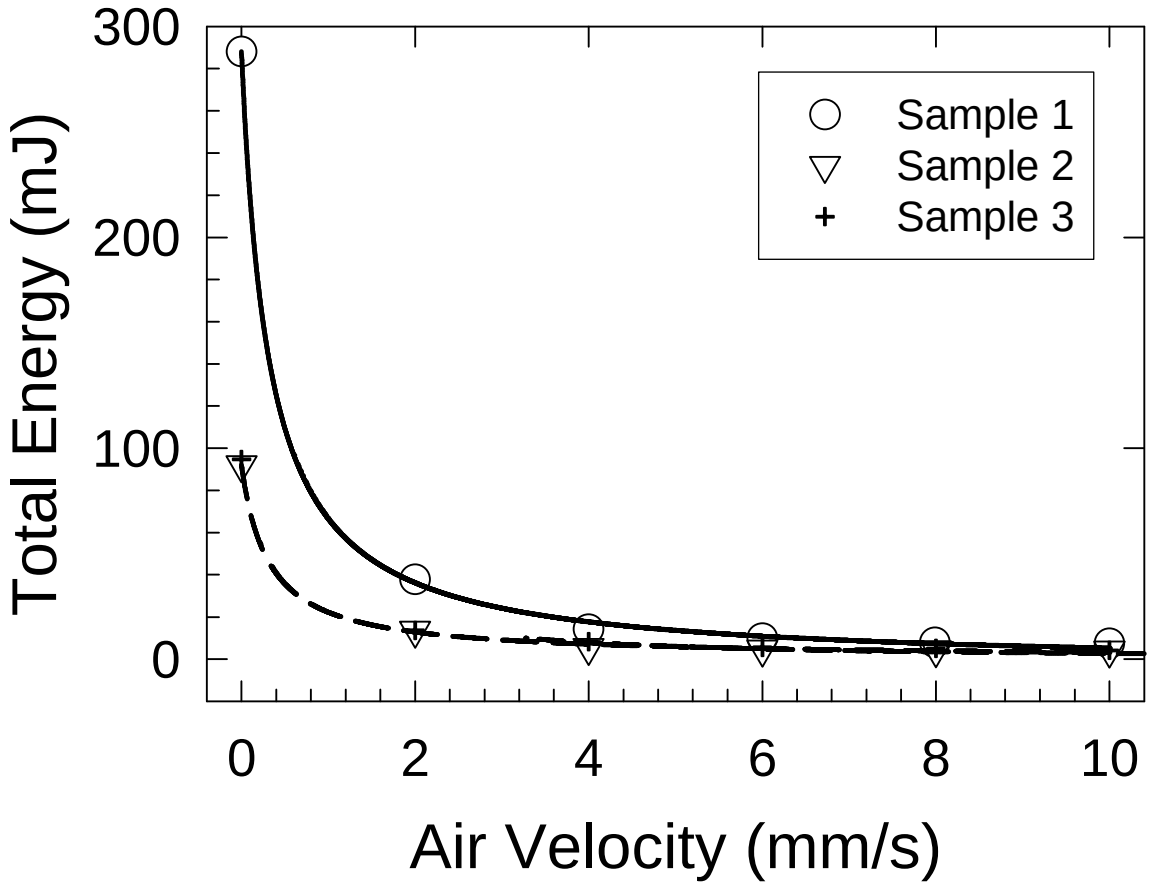

Figure 5. Aeration test results for studied mica powders (measured at 24 °C).

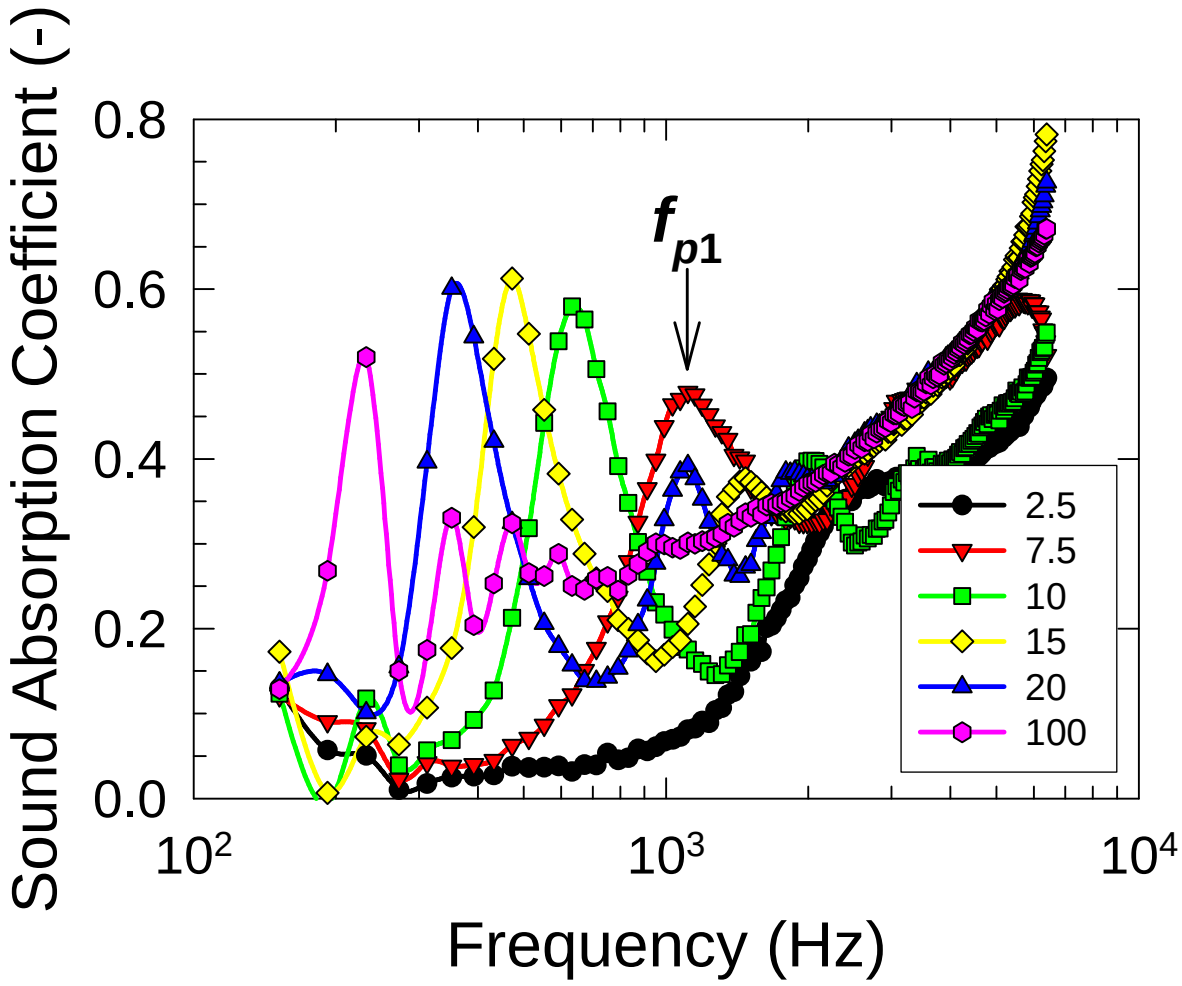

Figure 6. Sound absorption coefficient frequency dependence of the mica powder sample 2 as observed for different loose unconsolidated powder layer thickness given in millimetres (see the insert legend). (For interpretation of the references to colour in this figure legend, the reader is referred to the web version of this article).

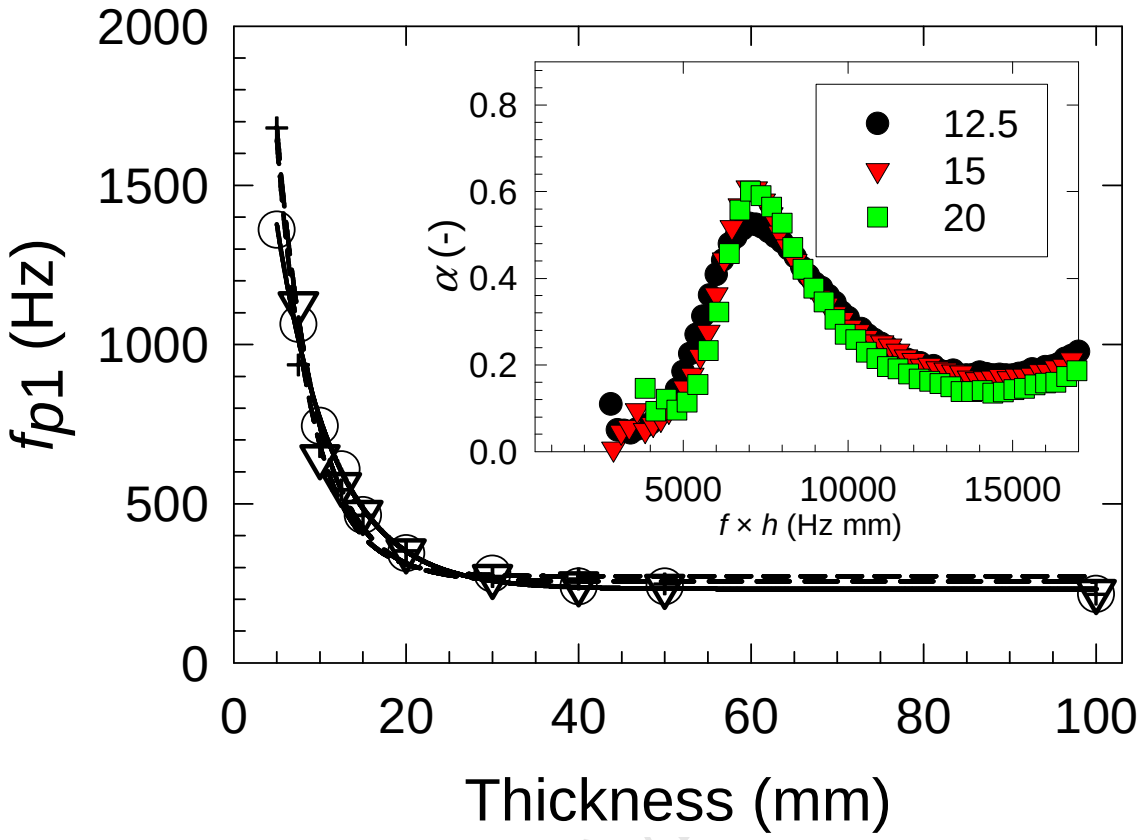

Figure 7. Dependence of the primary absorption peak frequency (f_{p1}) vs. loose powder layer thickness of the studied mica powders: sample 1 (circle), sample 2 (triangle) and sample 3 (crosshair). Inset: Illustration for sample 2 of the sound absorption coefficient (α) dependence on product of frequency × thickness ($f \times h$) being constant irrespective of specimen thickness. Inserted inset legend: loose powder thickness in millimetres. (For interpretation of the references to colour in this figure legend, the reader is referred to the web version of this article).

Highlights

- Correlation of surface energy analysis and powder rheology with the acoustical performance of the studied mica powders was presented.
- There was determined yield locus and Mohr´s circles of the mica powders.
- The worst sound absorption performance was found for the highest packing density material.